Materials Chemistry and Physics 277 (2022) 125553

Contents lists available at ScienceDirect

Materials Chemistry and Physics

journal homepage: www.elsevier.com/locate/matchemphys

Computational evaluation of optoelectronic, thermodynamic and electron transport properties of $CuYZ_2$ (Z= S, Se and Te) chalcogenides semiconductors

Mohammed Elamin Ketfi [a,b,*], Hamza Bennacer [a,b], Saber Saad Essaoud [c,d], Mohamed Issam Ziane [e], Abdelkader Boukortt [b]

[a] Department of Electronics, Faculty of Technology, University of M'sila, 28000, M'sila, Algeria
[b] Elaboration and Physical, Mechanical and Metallurgical Characterization of Materials Laboratory, ECP3M, Electrical Engineering Department, Faculty of Sciences and Technology, University of Mostaganem, 27000, Algeria
[c] Department of Physics, Faculty of Science, University of M'sila, 28000, M'sila, Algeria
[d] Laboratoire de Physique des Particules et Physique Statistique, Ecole Normale Supérieure-Kouba, BP 92, Vieux-Kouba, 16050, Algiers, Algeria
[e] The Higher School in Electrical and Energetic Engineering (ESGEE), 31000, Oran, Algeria

HIGHLIGHTS

- $CuYZ_2$ (Z = S, Se and Te) chalcogenides compounds are semiconductors.
- $CuYS_2$ compound has a high optical absorption coefficient compared to the other compounds.
- At room temperature, $CuYS_2$ compound has a higher heat capacity "C_v" and lower thermal expansion.
- Unlike the $CuYTe_2$ compound, the highest ZT factor value was obtained for both $CuYS_2$ and $CuYSe_2$.
- The results advocate using this material for photovoltaic and thermoelectric applications.

ARTICLE INFO

Keywords:
TB-mBJ
Seebeck coefficient
Electrical and thermal conductivity coefficients
Dielectric function
Absorption coefficient
Reflectivity
Heat capacity
Thermal expansion coefficient

ABSTRACT

Due to their useful physical properties, copper-based chalcogenides materials are recently promising for numerous emerging technological fields. In photovoltaics, discovering and designing suitable materials for solar cells is a primary technical challenge. The structural, electrical, optical, and thermoelectric properties for both $CuYSe_2$ and $CuYTe_2$ in the hexagonal phase, as well as $CuYS_2$ in the orthorhombic phase have been investigated using a numerical Full Potential-Linearized Augmented Plane Wave (FP-LAPW) technique based on Density Functional Theory (DFT).

To compute the structural properties, both, the local density approximation (LDA) and the generalized gradient approximation (PBE-GGA) were used as exchange-correlation potentials. On the other hand, the modified Becke-Johnson (mBJ) was used to compute the optoelectronic, properties with higher degree of precision. Our calculations revealed that these three compounds have indirect band gaps in the range of 0.6 eV–2.1 eV. Moreover, numerous thermoelectric qualities of the investigated compounds estimated as a function of chemical energy at different temperatures using the semi-local Boltzmann transport theory, whereby the findings exhibit a higher Seebeck coefficient for $CuYS_2$ compared to $CuYZ_2$(Z = Se and Te) up to 2.7 mV/K for $CuYS_2$ at 300 K, with acceptable values of thermal and electronic conductivity. The quasi-harmonic model is used to examine thermodynamic properties such as heat capacity at constant pressure and volume, entropy, Debye temperature, and thermal expansion coefficient under both pressure and temperature influences. As a result of this study, $CuYS_2$, $CuYSe_2$ and $CuYTe_2$ are promising materials for optoelectronic devices, especially as photovoltaic materials in solar cells.

* Corresponding author. Department of Electronics, Faculty of Technology, University of M'sila, 28000, M'sila, Algeria.
E-mail addresses: mohammedelamin.ketfi@univ-msila.dz, medketfi5@gmail.com (M. Elamin Ketfi).

https://doi.org/10.1016/j.matchemphys.2021.125553
Received 7 August 2021; Received in revised form 21 October 2021; Accepted 7 December 2021
Available online 10 December 2021

1. Introduction

Finding and developing suitable materials for photovoltaic cells is a major technical issue in solar technology. A promising photovoltaic absorber must have an appropriate band gap for solar cells, high optical absorption, non-toxic and abundant materials [1]. Experimental [2–7] and theoretical prediction [7–12] research for optoelectronic and photovoltaic materials used to refine and improve the device's performance and contribute to discovery a large number of compounds, which, differ in terms of material cost, toxicity, stability of their structural and electronic properties, as well as their ability to interact effectively with light, since their optical properties respond to the light intensity exposed to. Due to their semiconducting behavior and their useful physical properties, copper-based chalcogenides materials in chalcopyrite, chalcostibite, emplectite, kesterite and stannite structures are recently considered as promising materials for numerous emerging technological fields, including optoelectronic and photovoltaic devices [13–18]. Thin-film solar cells have become more practical and commercially viable indeed for recent advancements in copper indium gallium selenide Cu(Ga,In)Se_2, the material used to make the best thin-film solar cells [4]. Furthermore, Jiang et al. [2] showed that copper-based chalcopyrite is one of the best materials in high-efficiency thin films solar cells application. Also, Ting et al. [19] showed in their study the possibility of applying copper ternary chalcogenides as 2D materials due to their a good bandgap (where the energetic gap was equal to 1.53 eV, 1.38 eV and 0.99 eV for $CuInS_2$, $CuSbS_2$ and respectively $CuInSe_2$) that enabled to endowed various applications in electronics, optoelectronics. Moreover, Sorina et al. [3] demonstrated experimentally that copper-based chalcogenide has good thermoelectric properties, with the possibility to obtain multilayer structures, these films could be used as thin-film based thermoelectric devices.

Another endeavor in the study of solid materials, especially semiconductors, is to verify if they are adequate for use in modern power source equipment where this last research axe is considered as one of the most important research challenges at the present time as this research mostly focuses on developing different ways of converting other renewable energies, especially electric energy.

Thermal energy is one of the most important sources of energy in our daily life due to the variety of resources available, including solar energy and waste heat generated by machines or motors that may be recovered and converted into electrical energy.

Thermoelectric generators are among the most efficient ways to recover and convert waste heating energy into electrical energy, this technology is based on the Seebeck effect, which was discovered in 1821 when Thomas Seebeck observed a voltage difference between the ends of two different materials exposed to two different temperatures. The thermoelectric properties of materials have recently received considerable attention and have become a priority for scientific research, as they are the basis for many renewable energy applications. Since these modern technologies in generating electric power are favored than the old technologies because they do not emit noise that's because they use non-moving materials and only depend in their principle work only on the intrinsic properties of semiconductor materials.

The suitability of using any material for usage as thermoelectric parts in devices whether they are generators or sensors is evaluated using the merit figure ZT $\left(ZT = \frac{S^2 \sigma T}{\kappa}\right)$ where this factor is controlled by several other parameters of the substance, such as the contribution of electrons to the electrical conductivity and thermal conductivity, as well as the Seebeck coefficient.

Ternary Cu-based chalcogenides compounds with $A^I B^{III} C_2^{IV}$ (A = Cu, B=Y and C= S, Se and Te) are among materials that had direct band gap energy and can be crystallized in several structures, these features have put this category of materials in a superior status, allowing them to be used in a wide range of technologies [5]. In recent years, an experimental study carried out by Li et al. [5] on the Copper Yttrium Selenide compound after its preparation and using X-ray diffraction showed that it has a good absorption capacity in the visible light range with bandgap of 1.53 eV, which is close to the optimum value to use in solar cells. In addition, the $CuYSe_2$ film with an I_{light}/I_{dark} ratio equal to 2.81 appeared an excellent photo-electron responsive behavior [5]. Since Cu-based chalcogenides are known by their stability, low cost and low toxicity, so we decided to study $CuYS_2$, $CuYSe_2$ and $CuYTe_2$ compounds in order to explore their structural, optoelectronic, thermodynamic and thermoelectric properties. Therefore, $CuYS_2$ in its orthorhombic phase, as well as $CuYSe_2$ and $CuYTe_2$ in the hexagonal structure, have been studied as part of the copper-based chalcogenide materials category, and hence, we provided details about the calculations we performed, and then analyzed and interpreted the results obtained for the structural, electronic, optical, thermodynamic and thermoelectric properties in the second part, and in the conclusion, we highlighted the most important conclusions that we extracted through this study.

2. Computational details

The Full Potential-Linearized Augmented Plane Wave (FP-LAPW) method based on the density functional theory (DFT) within the WIEN2k code [20] is used in this paper to predict the structural, optoelectronic, thermoelectric properties of $CuYS_2$, $CuYSe_2$ and $CuYTe_2$. We used both the local density approximation (LDA) [21] of Perdew and Wang and the revised Perdew-Burke-Ernzerhof (PBESol) parameterization of the generalized gradient approximation (GGA) [22] to treat exchange-correlation potential for the structural properties whereas the modified Becke-Johnson exchange potential [23] was used for the optoelectronic properties. The unit cell is divided into non-overlapping muffin-tin spheres and an interstitial region. In the interstitial region, the wave functions are expanded in terms of plane waves with a cut-off of $R_{MT}{*}K_{MAX} = 8$, where R_{MT} is the minimum muffin-tin radius and K_{MAX} gives the magnitude of the maximum K vector wave in the Brillouin zone. Whereas, a spherical harmonic expansion has used inside the spheres with an angular momentum up to $l_{max} = 10$. The chosen values of the muffin-tin radius R_{MT} for Cu, Y, S, Se and Te atoms are 2.15, 2.4, 1.75, 2.35 and 2.4 (a.u) respectively. For the Brillouin zone (BZ) integration, 162 special k-points have been used for $CuYS_2$ and 100 special k-points have been used for both $CuYSe_2$ and $CuYTe_2$ in the irreducible wedge, the electronic configurations for valence electrons are for Cu ($3d^{10}\,4s^1$), Y ($4d^1\,5s^2$), S($3s^2\,3p^4$) Se ($3d^{10}\,4s^2\,4p^4$) and Te ($4d^{10}\,5s^2\,5p^4$). To separate between the valence and core states −6 eV was used as separating energy. Both energy (10^{-5} Ry) and charge (10^{-3} e) values were used as criteria for convergence during the calculation. To appear pressure and temperature effects on different thermal properties, we employed the quasi-harmonic model implemented in the GIBBS2 code [24,25]. To estimate the thermoelectric properties, we have used the semi-local Boltzmann transport theory implemented in BoltzTraP code [26].

3. Results and discussion

3.1. Structural properties

Ternary chalcogenides with copper-based can be crystallized in several types of structures, which directly affect many properties, especially electronic and optical. For this reason, we studied $CuYS_2$ compound in orthorhombic phase structure with *Pnma* space group (62) and $CuYSe_2$, $CuYTe_2$ in hexagonal phase with *P-3m1* space group (164) (see Fig. 1). Before calculating lattice constants, bulk modulus and the cohesive energy, we should determine the atoms positions formed these compounds, through full geometry optimizations, the internal atomic positions are relaxed by using the total energy and force minimization scheme basing on Broyden's method [27,28] in which a good relaxed

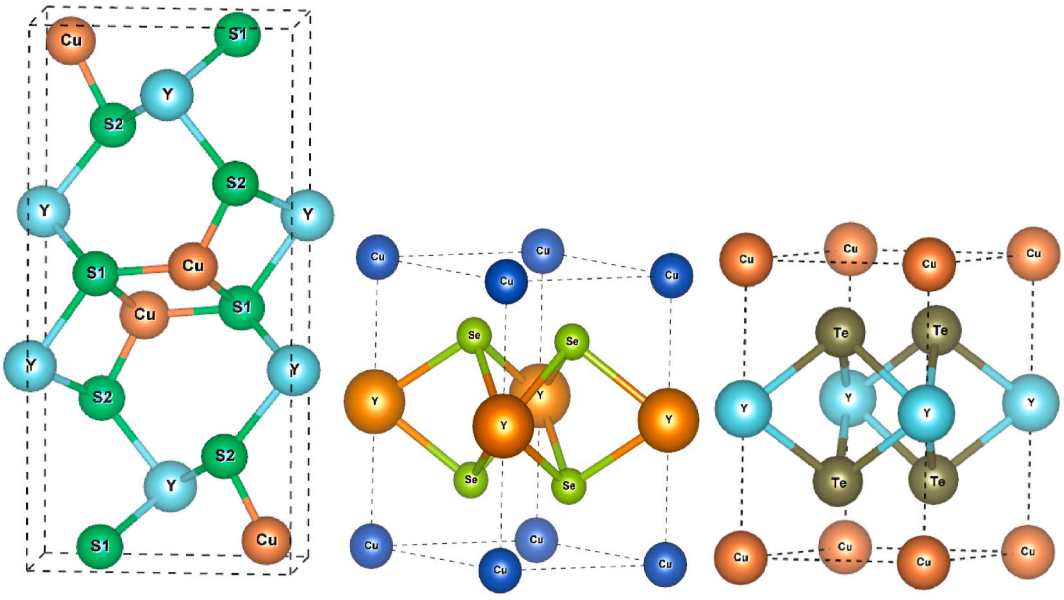

Fig. 1. Crystal structure of: (a) $CuYS_2$ (orthorhombic), (b) $CuYSe_2$ and (c) $CuYTe_2$.

structure can be achieved if the force applied to each atom was smaller than 0.5 Ry/au. The optimized positions of the atoms for each compound by using GGA and LDA approximations are presented in Table.1 and compared to other experimental or theoretical results. Computing the lattice parameter "a" of each unit cell is performed by calculating the total energy at different volumes, and then, we use the Murnaghan equation of state [29] to determine the equilibrium volume that correspond to the lowest energy (see Fig. 2). Thereafter, the total energy for different values of c/a ratio for the hexagonal as well as c/a and then b/a for the orthorhombic structure at a fixed volume is computed to measure the lattice constant "c" for both $CuYSe_2$ and $CuYTe_2$ in the hexagonal phase, as well as "b" and "c" constants in the orthorhombic phase for $CuYS_2$.

The equilibrium lattice constants, bulk modulus, and cohesive energy are calculated and denoted summarized in Table 2 and compared with the other available results, from this table we can see that the finding lattice parameters obtained using GGA approximation for $CuYS_2$ and $CuYTe_2$ compounds are in good agreement with the other experimental results, whereas the nearest parameters of the experiment results for the $CuYSe_2$ compound are obtained using LDA approximation. The bulk modulus *B*(GPa) describes the material's resistance to any deformation caused by applying external hydrostatic pressure. Therefore, the bulk modulus values reveal that the $CuYS_2$ compound is more resistant against regular external pressure compared to $CuYSe_2$ and $CuYTe_2$ where this distinction is attributed to a disparity in the number of bonds, the strength of these bonds between atoms and the difference in structure type between $CuYS_2$ and the remaining compounds. We can confirm this result by calculating the cohesive energy of these compounds according to the following formula:

$$E_{coh} = \frac{\left(E_{atom}^{Cu} + E_{atom}^{Y} + 2\ E_{atom}^{Z}\right) - E_{tot}^{CuYZ_2}}{N_{Cu} + N_Y + N_Z} \quad (1)$$

where N_{Cu}, N_Y and N_Z are the numbers of Cu, Y and Z atoms, respectively, in the unit cell of the $CuYZ_2$ compound and E_{atom}^{Z} are isolated atoms energies of the Cu, Y and Z atoms, respectively, $E_{tot}^{CuYZ_2}$ is the total energy of bulk $CuYZ_2$ compound. Comparing the cohesive energy of these compounds leads to finding that the $CuYS_2$ is more cohesive because it has higher energy and is, therefore, the most structurally stable.

3.2. Electronic properties

Knowing the electronic behavior of materials has a great importance

Table 1
Calculated atomic positions using GGA and LDA approximations of $CuYZ_2$ (Z = S, Se and Te) compounds.

		GGA			LDA			Other works		
Materials	Atoms	x	y	z	x	y	z	x	y	z
$CuYS_2$ (Pnma # 62)	Cu	0.4561	0.2500	0.3758	0.4589	0.2500	0.3768	0.4465	0.2500	0.3919 [30]
	Y	0.1335	0.2500	0.5016	0.1336	0.2500	0.5013	0.1348	0.2500	0.4925 [30]
	S	0.4602	0.2500	0.7534	0.4621	0.2500	0.7514	0.4623	0.2500	0.7597 [30]
	S	0.2965	0.2500	0.2418	0.3002	0.2500	0.2440	0.2934	0.2500	0.2310 [30]
$CuYSe_2$ (P-3m1 # 164)	Cu	0.0000	0.0000	0.0000	0.0000	0.0000	0.0000	–	–	–
	Y	0.0000	0.0000	0.5000	0.0000	0.0000	0.5000	–	–	–
	Se	0.3333	0.6666	0.2323	0.3333	0.6666	0.2500	–	–	–
	Se	0.6666	0.3333	0.7676	0.6666	0.3333	0.7500	–	–	–
$CuYTe_2$ (P-3m1 # 164)	Cu	0.0000	0.0000	0.0000	0.0000	0.0000	0.0000	–	–	–
	Y	0.0000	0.0000	0.5000	0.0000	0.0000	0.5000	–	–	–
	Te	0.3333	0.6666	0.2245	0.3333	0.6666	0.2246	–	–	–
	Te	0.6666	0.3333	0.7754	0.6666	0.3333	0.7753	–	–	–

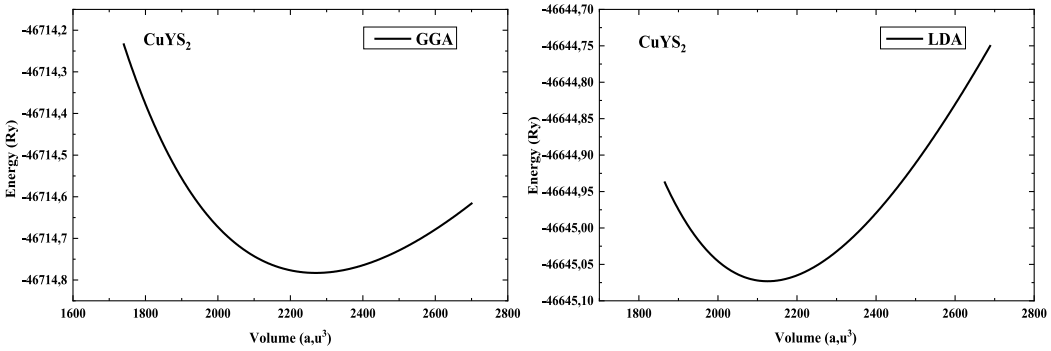

(a)

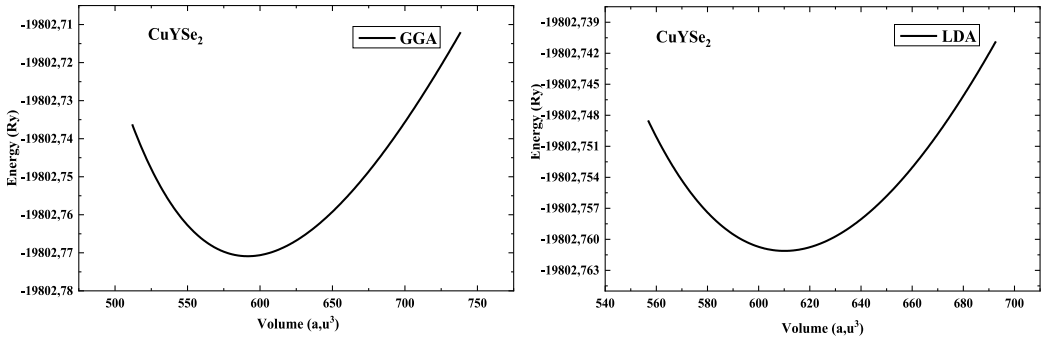

(b)

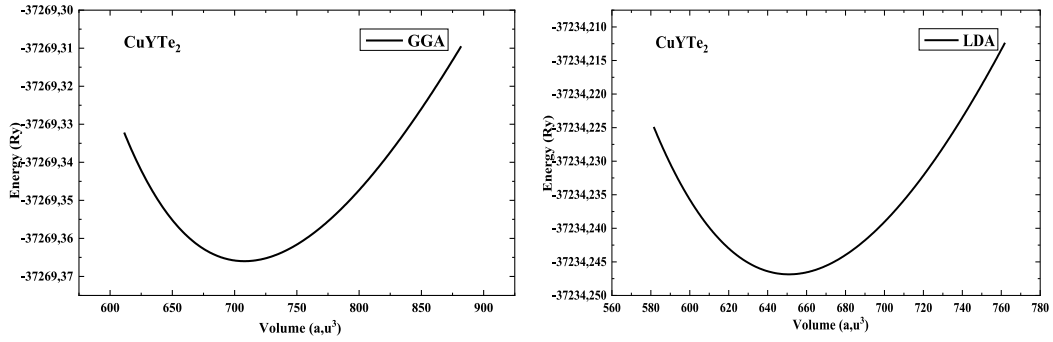

(c)

Fig. 2. Energy-Volume optimization curves for (a) $CuYS_2$ (b) $CuYSe_2$ (c) $CuYTe_2$ compounds.

in technology because it allows us to decide the appropriate domain for their use. The majority of chalcogenide compounds have semiconductor behavior, as proven in several studies [32]. Due to this character, these compounds are high demand, especially in the spintronic and solar cells fields. The band structure and the states densities using the TB-mBJ approach are plotted in Figs. 3–5.

Band structures curves of the studied compounds indicates the presence of two bands (conduction above Fermi level and valence below) separated from each other by an indirect gap, where the value of the gaps estimated using TB-mBJ approximation are 2.01, 1.35 and 0.64 eV for $CuYS_2$, $CuYSe_2$ and $CuYTe_2$ respectively, and therefore we can say that these three compounds have semiconductor behavior. We notice that our results are in good agreement with the other experiment work [11,12]. To understand the formation of each band in band structure spectra, we analyze the total and the partial density of the atomic orbitals states that shown in Fig. 3. According to this figure, we notice that there is no density of the state around the Fermi level, which confirms the semiconductor behavior of these compounds. Also, for $CuYS_2$ in its orthorhombic phase structure, it is clear that the conduction band is formed mainly by the dominant contribution of the "d" orbitals of the Yttrium atom, with the presence of weak contribution from "s" and "p" orbitals of Cu and Y atoms while the "d" and "p" orbitals of the Cu and S atoms respectively which they exhibit a strong hybridization in the range of −5 eV–0 eV, on the other hand, the contribution of "s" orbital of "S" atom was located around −12 eV. Partial density of states (PDOS) curves of $CuYSe_2$ and $CuYTe_2$ compounds have appeared that the valence band below Fermi level was formed due to "s" orbital of Se and Te atoms contribution near to −12 eV energy value, while "p" orbital of Se and Te atoms has contributed in the range [−5; 0 eV] and hybridized with "d" orbital of Cu atoms. For the conduction band, the partial density curves for both $CuYSe_2$ and$CuYTe_2$, appears a dominant contribution of "d" orbital of Y atoms. Through total partial density of

Table 2
The Calculated equilibrium lattice constants, bulk modulus, and cohesive energy for $CuYZ_2$ (Z = S, Se and Te) using both GGA and LDA approximations.

		a (Å)	b (Å)	c(Å)	B (GPa)	E_{coh} (eV/atom)
$CuYS_2$	GGA	13.446	3.979	6.287	80.594	4.868
	Other cal [11]	13.758	4.013	6.351	73.48	–
	LDA	13.154	3.892	6.151	97.195	6.251
	Other cal [11]	13.196	3.858	6.111	84.37	–
	Exp [30]	13.453	3.981	6.290	–	–
$CuYSe_2$	GGA	3.995		6.339	71.180	4.305
	Other cal [11]	3.994		6.372	–	–
	LDA	4.037		6.405	66.999	6.556
	Exp [31]	4.068		6.454	–	–
$CuYTe_2$	GGA	4.223		6.748	57.119	3.874
	Other cal [7]	4.317		6.918	–	–
	LDA	4.107		6.587	73.457	5.267
	Exp [7]	4.297		6.908	–	–

states analysis, our obtained results are similar to the previous studies [11,12].

3.3. Optical properties

The effect of incident light on solid materials differs depending on their electronic behavior (conductor, insulator, or semiconductor), electronic density, and the gap separating the valence bands from the conduction, and the number and the nature of bonds between their atoms. For semiconductor materials, this difference is mainly due to the value of the energy carried by the electromagnetic waves, the photon-electron interaction and valence band electrons, where the electric field of the electromagnetic waves interacts with electrons and polarizes them in its same direction. As a result of this polarization, the light energy can be absorbed through the excitation of the valence electrons, in which this polarization gives sufficient energy to the electrons that allows them to move from the valence band to the conduction band in the so-called interband transition, where the excited electrons, the energy range in which the interband transition occurs, and the atomic orbital to which they transform to/or from can be inferred and determined depending on the electronic state density analysis. These phenomena can be depicted in terms of time-dependent perturbations of the ground-state electronic states. As another result of the polarization, the velocity of these electromagnetic waves can be reduced when across the material, where the refraction of the light occurs and its path changes. Absorption, reflection, refractive index, and energy loss coefficients are among the main characteristics that indicate usability of material in a specific application, whether as optical filters, optical detectors, sensors, or anti-reflection coatings.

The optical properties were studied using the dielectric complex function $\varepsilon(\omega)$ as a function of real ($\varepsilon_1(\omega)$) and imaginary ($\varepsilon_2(\omega)$) parts given by the formula [33–36]:

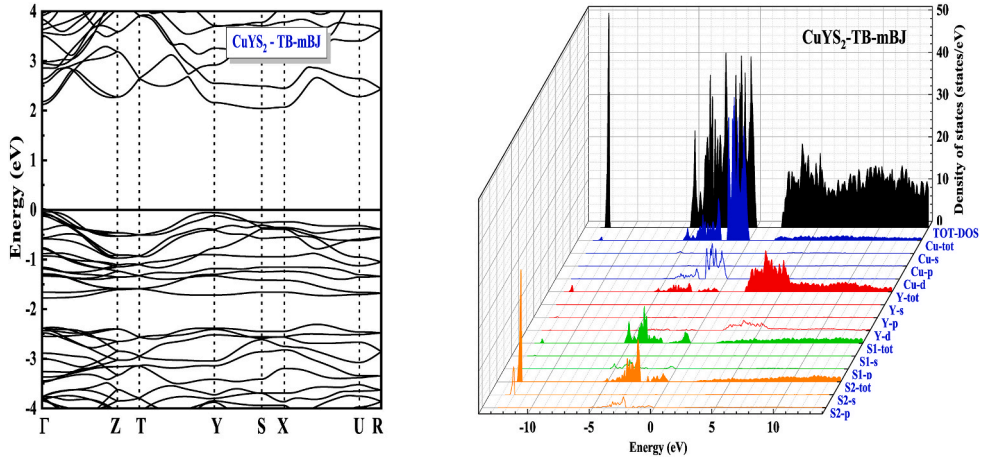

Fig. 3. Calculated band structure, total and partial density of states for $CuYS_2$ by using the TB-mBJ approximation.

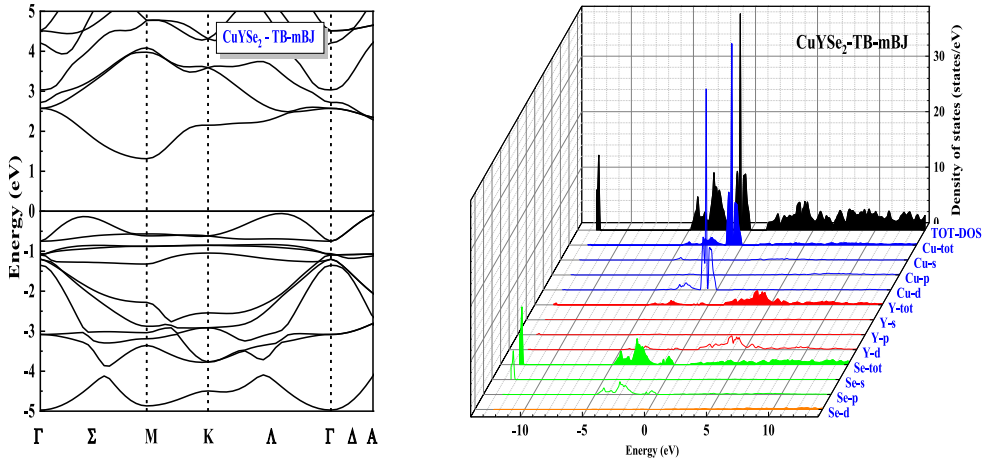

Fig. 4. Calculated band structure, total and partial density of states for $CuYSe_2$ by using the TB-mBJ approximation.

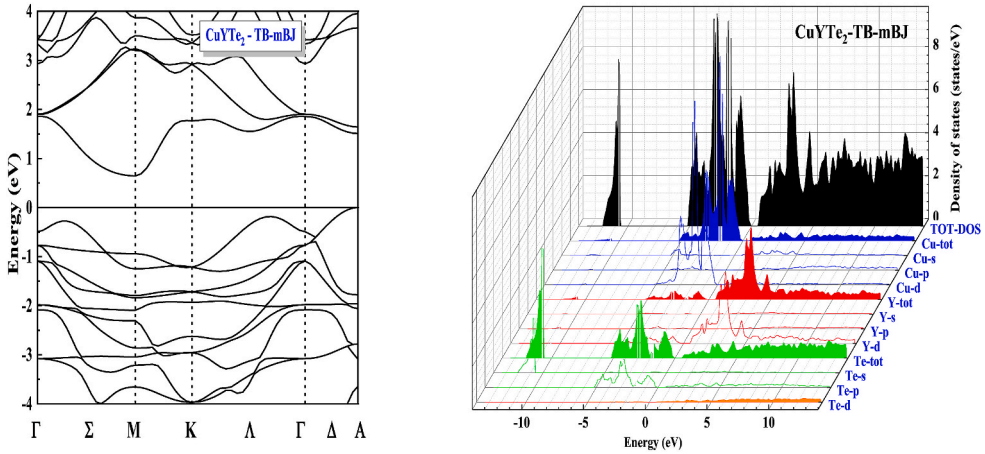

Fig. 5. Calculated band structure, total and partial density of states for $CuYTe_2$ within the TB-mBJ approximation.

$$\varepsilon(\omega) = \varepsilon_1(\omega) + i\varepsilon_2(\omega) \quad (2)$$

The real part of the dielectric function $\epsilon_1(\omega)$ present the dispersion of the incident photons by the substance's [37] and it gives us more information about the electronic polarization state of the material [38] while the imaginary part of the dielectric function $\epsilon_2(\omega)$ means the energy absorbed by the material. The Imaginary part $\epsilon_2(\omega)$ is estimated using the electronic band structure by relating the momentum matrix elements between the occupied and unoccupied electronic states [39] whereas the real part can be obtained from the Imaginary part $\epsilon_2(\omega)$ using the Kramers–Kronig transformation [40].

The real and imaginary parts of the dielectric functions of the studied compounds are calculated using TB-mBJ approximation along each x, y, and z directions and presented in Figs. 6 and 7. Through this figures, we can see that the values of the real part $\epsilon_1(\omega)$ at zero frequency present the static dielectric constant which are calculated and summarized in Table 3 where we can see reveals that $CuYTe_2$ has a higher value compared to the other compounds. Also, we can observe that the spectra of $\epsilon_1(\omega)$ increase sharply from the static dielectric constant $\epsilon_1(0)$ and reaches its maximum value at energies equal to 10.5, 9.0 and 7.0 eV for $CuYS_2$, $CuYSe_2$ and $CuYTe_2$ respectively, since then gradually decreases to take negative values in the range [8; 18 eV] for all the studied compounds where their behavior in this region they transform from metallic to dielectric and therefore the dispersion is unavailable in this range, unlike to the absorption coefficient, which has a greater value in this range.

Regarding the spectra of the imaginary part ϵ_2 (ω) plotted in figures (6 and 7), we can see that the optical band gaps obtained from the imaginary part of the dielectric function calculated using TB-mBJ approximation are 2.01, 1.31 and 0.56 eV for $CuYS_2$, $CuYSe_2$ and $CuYTe_2$ respectively. The ϵ_2 (ω) spectra express the absorption that can occur as a result of electronic excitation from the valence states below the Fermi level to the conduction states where through this spectra we can observe that this absorption can only occur if the energy value of the incident photons is greater than the energy gap.

The light incidence as an electromagnetic waves on the material causes electrons in the valence band to absorb the energy and raising its energy level [41]. The absorption coefficient α(ω) is connected to the extinction coefficient k(ω), by the following formula [40].

$$\alpha(\omega) = (4\pi/\lambda)\mathrm{k}(\omega) \quad (3)$$

where λ is the wavelength of light in vacuum. Also the absorption coefficient α(ω) can be calculated using another formula [40]:

$$\alpha(\omega) = \frac{2\pi\omega}{c}\sqrt{\frac{-R_e(\varepsilon(\omega)|\varepsilon(\omega)|)}{2}} \quad (4)$$

According to Fig. 8, the absorption edge is located at around 2.04 eV for $CuYS_2$, 1.31 eV for $CuYSe_2$ and 0.56 eV for $CuYTe_2$ where all the studied compounds have a good response in the range of 11.3–47 eV for $CuYS_2$, 6.25–47eV for $CuYSe_2$ and 5.7–47 eV for $CuYTe_2$ to incident photons.

The optical refractive index, conductivity and the reflectivity are presented in Figures (9)–(11). We have determined the refractive index given by using the real and imaginary parts of the dielectric function [40]:

$$n(\omega) = \left(1/\sqrt{2}\right)\left[\sqrt{\varepsilon_1(\omega)^2 + \varepsilon_2(\omega)^2} + \varepsilon_1(\omega)\right]^{1/2} \quad (5)$$

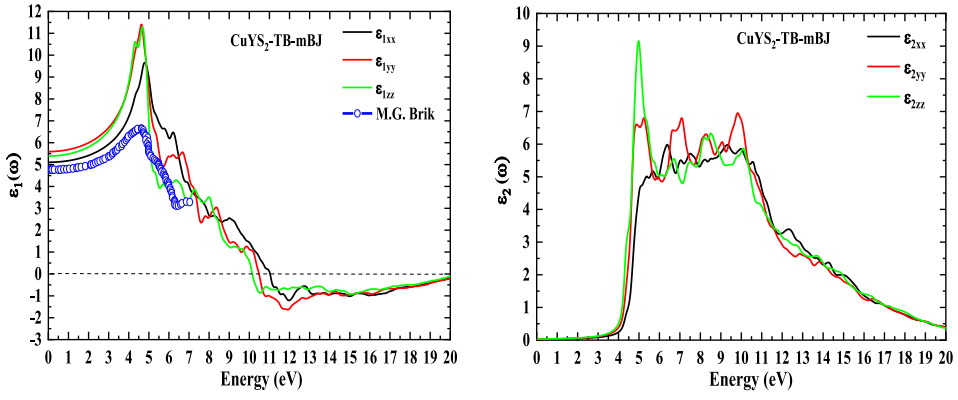

Fig. 6. Real and imaginary part of the dielectric function for $CuYS_2$ within TB-mBJ approximation compared the real one with other computational work.

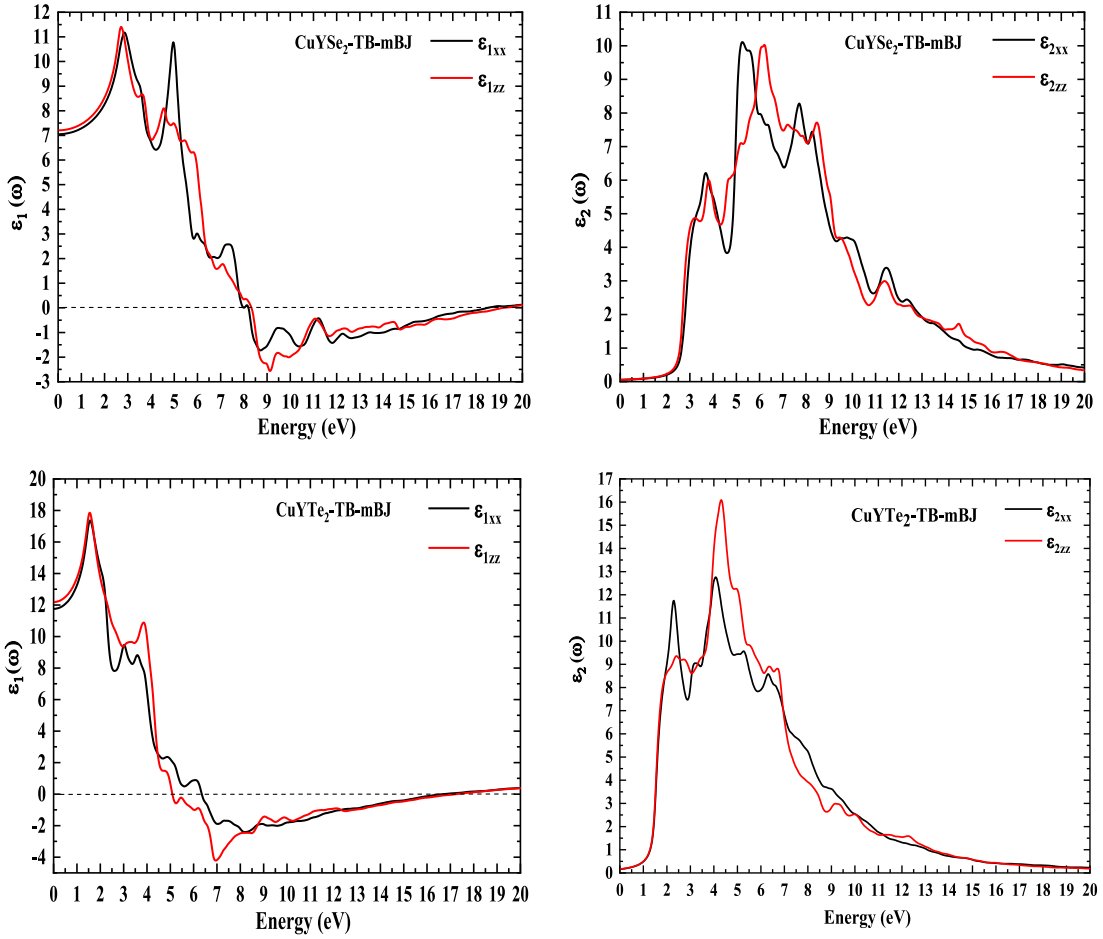

Fig. 7. The computed real and imaginary part of the dielectric function for $CuYSe_2$ and $CuYTe_2$ within TB-mBJ approximation.

Table 3
The values of the refractive index and the static dielectric constant.

		$\varepsilon_1(0)$	$n(0)$	$R(0)$
$CuYS_2$	mBJ-GGA	4.942	2.22	0.144
	mBJ-LDA	5.105	2.26	0.149
$CuYSe_2$	mBJ-GGA	7.632	2.76	0.219
	mBJ-LDA	7.048	2.65	0.205
$CuYTe_2$	mBJ-GGA	11.754	3.42	0.301
	mBJ-LDA	13.200	3.63	0.323

The refractive index n_0 at zero frequencies and the maximum values are shown in Table 3. At zero-frequency, the refractive index is 1.91 for $CuYS_2$, 1.88 for $CuYSe_2$ and 1.98 for $CuYTe_2$ with maximum values of 2.80 at 6.59 eV for $CuYS_2$, 2.92 at 7.90 eV for $CuYSe_2$ and 3.12 at 6.81eV for $CuYTe_2$ respectively.

We define another parameter, which is the reflectivity coefficient R (ω). This parameter characterizes the part of the reflected energy from the solid surface and can be derived by the refractive index [40] as follows:

$$R(\omega) = \left| \frac{(n(\omega)-1)^2 + k(\omega)^2}{(n(\omega)+1)^2 + k(\omega)^2} \right| \quad (6)$$

In Fig. 10, the optical reflectivity of $CuYZ_2$ (Z = S, Se and Te) was plotted as function of the light energy where the zero-frequency reflectivity limit of $CuYZ_2$ is found to be 0.14 for $CuYS_2$, 0.21 for $CuYSe_2$ and 0.30 for $CuYTe_2$. We can see also that the high reflectivity peaks are observed at energies 15.76 eV, 9.03 eV and 11.16 eV for $CuYS_2$, $CuYSe_2$ and $CuYTe_2$ respectively.

Optical conductivity is a complex quantity defined by the following formula [35]:

$$\sigma(\omega) = -(i\omega/4\pi)\varepsilon(\omega) \quad (7)$$

Fig. 11 shows that the optical conductivity starting from 2.04 eV, 1.31 eV and 0.56 eV to $CuYS_2$, $CuYSe_2$ and $CuYTe_2$ respectively. As remark, the maximum of optical conductivity of the compounds is at 10.57 eV for $CuYS_2$, 8.28 eV for $CuYSe_2$ and 6.62 eV for $CuYTe_2$.

3.4. Thermodynamic properties

Getting high efficiency for materials that used in solar energy systems requires the full knowledge of their properties such as the various changes occurred to their properties when under temperature and pressure effects. The most important characteristics that we studied included the changes in their energy absorption ability, their thermal expansion coefficient, and the resistance to deformation and other properties.

All these properties were theoretically investigated in a temperature range of up to 1000 K and under the pressure influence up to 30 GPa. It calculation was performed using the quasi-harmonic Debye model [33] applied in the GIBBS2 code [34,35].

To study the thermodynamic properties variation of a solid matter under the influence of temperature and pressure, we use the Gibbs free energy given by:

$$G^*(x, V; P, T) = E_{stat}(x, V) + PV + A^*_{vib}(x, V; T) + F^*_{el}(x, V; T) \quad (8)$$

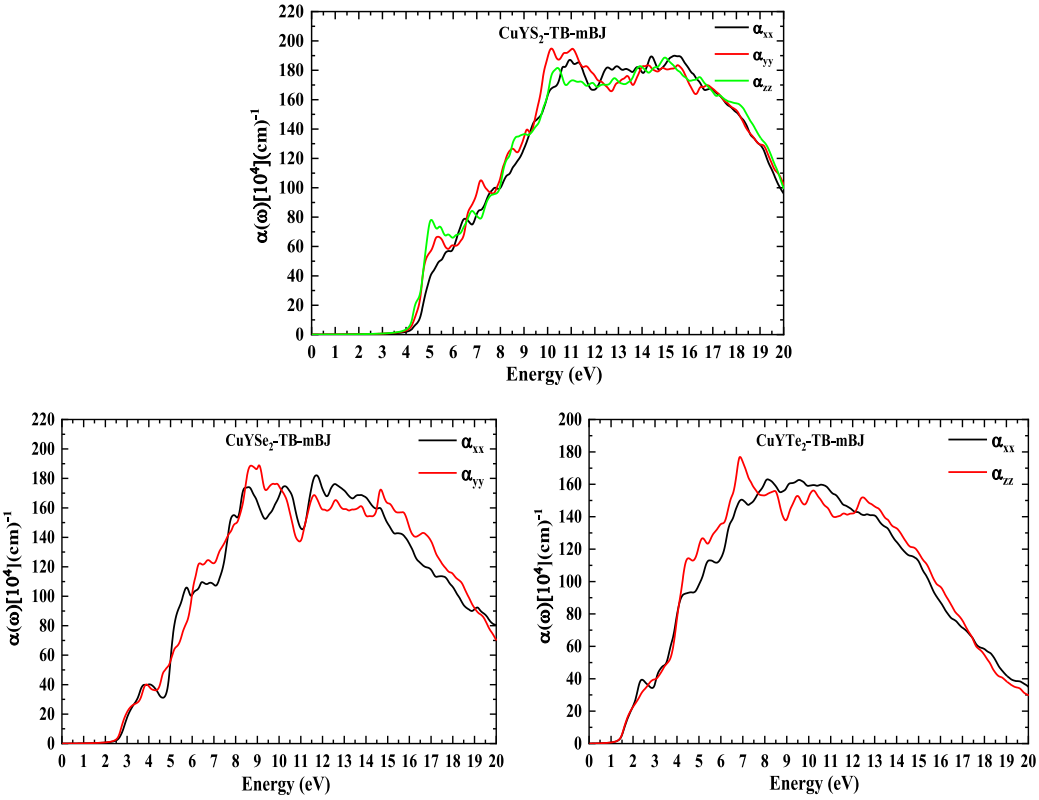

Fig. 8. Absorption coefficient of $CuYZ_2$ (Z = S, Se and Te) within TB-mBJ approach.

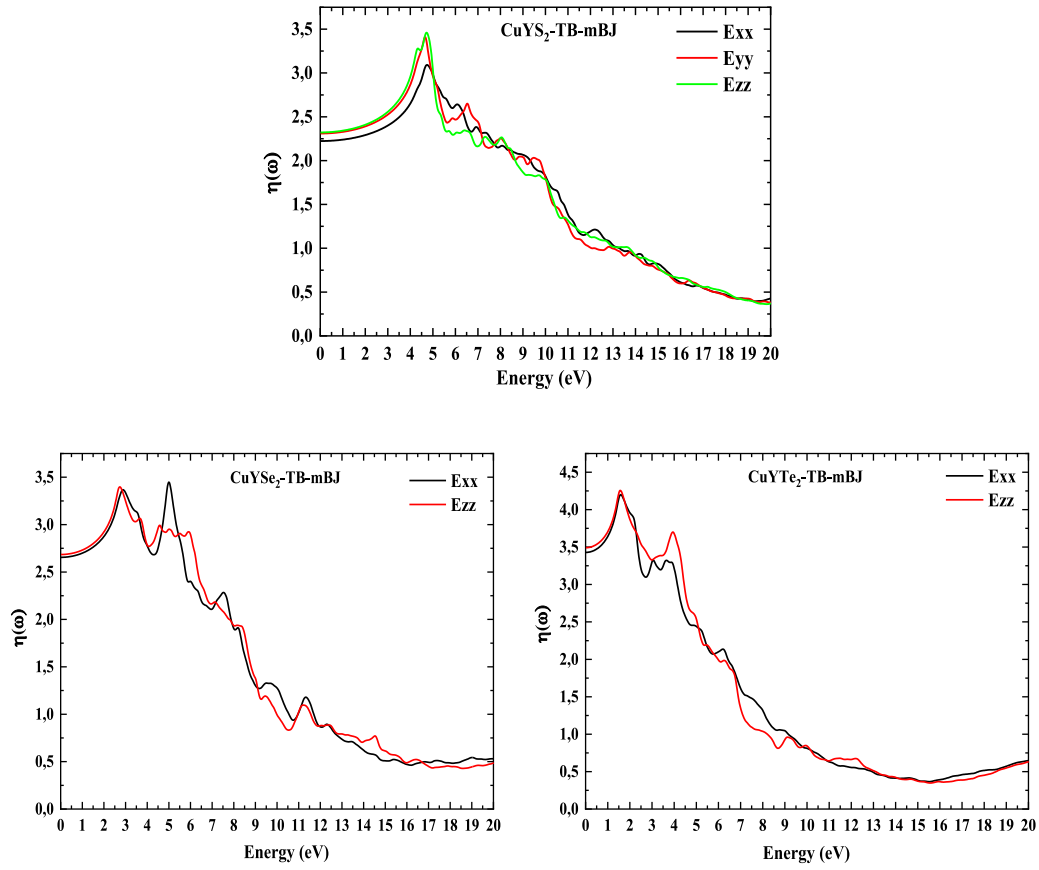

Fig. 9. Optical refractive index of $CuYTe_2$ with (Z = S, Se and Te) within TB-mBJ approach.

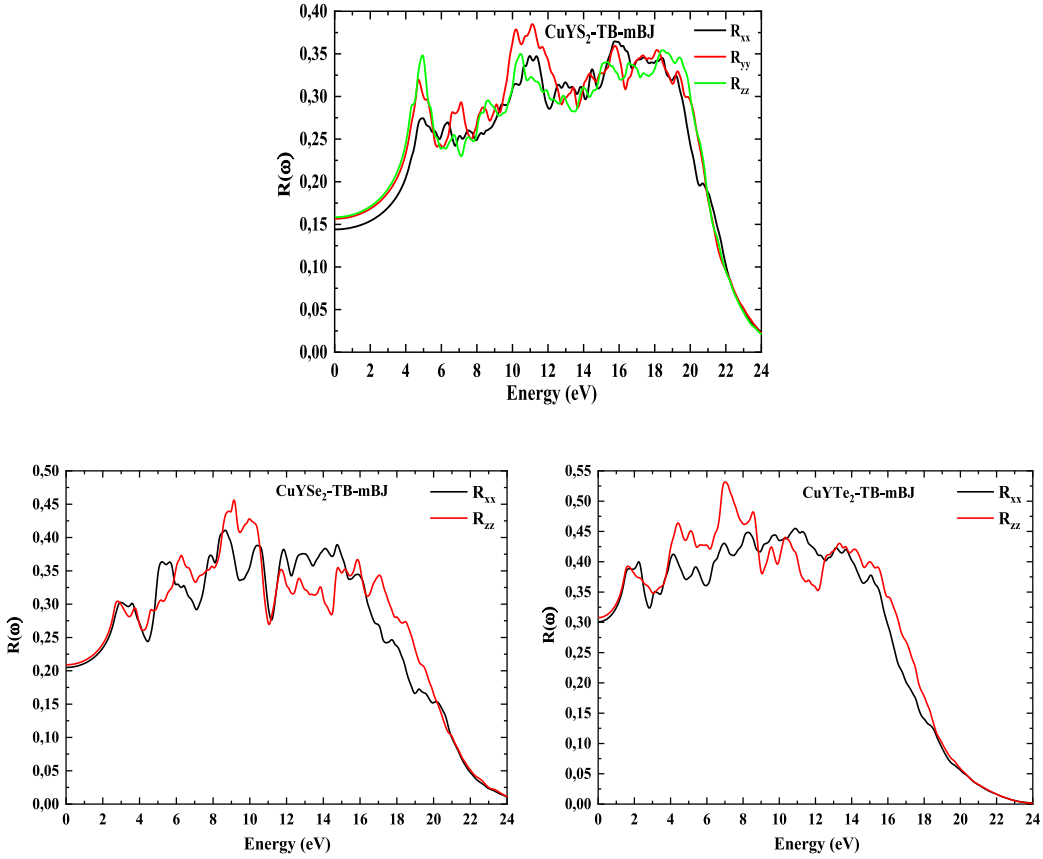

Fig. 10. Optical reflectivity of $CuYZ_2$ with (Z = S, Se and Te) using TB-mBJ approach.

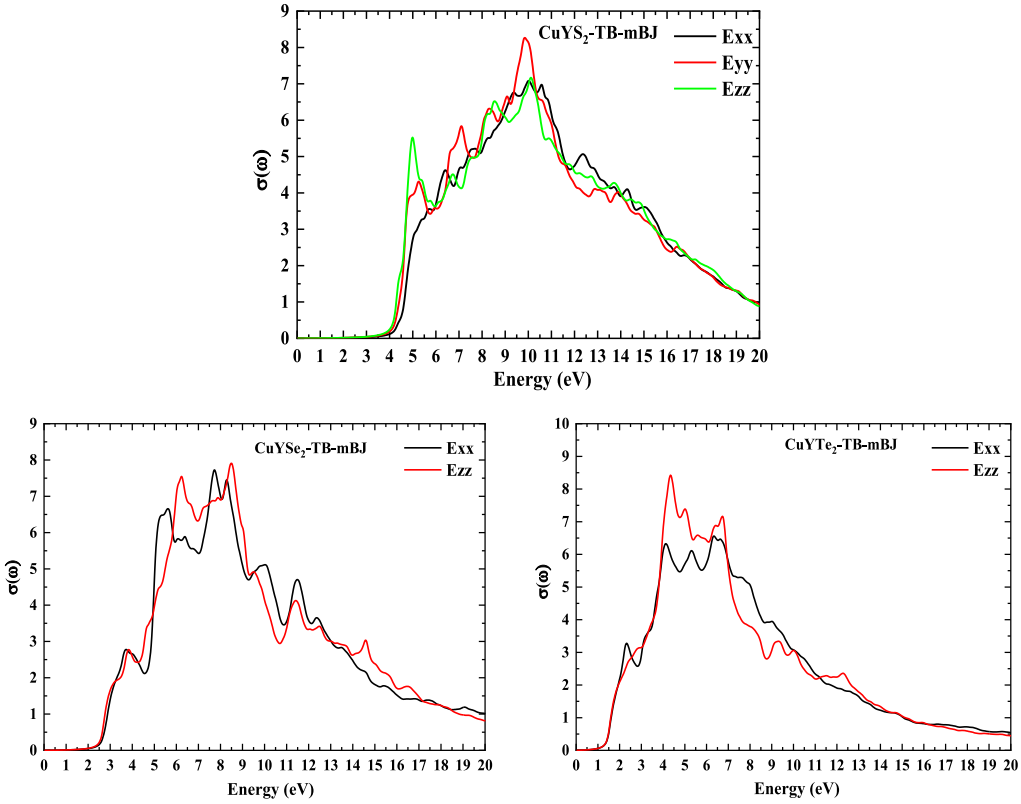

Fig. 11. Optical conductivity of $CuYZ_2$ (Z = S, Se and Te) using TB-mBJ approach.

where E_{stat} is the total energy, PV corresponds to the hydrostatic condition, A^*_{vib} and F^*_{el} are the non-equilibrium vibrational Helmholtz free energy and electronic free energies respectively. Using Debye's model allows to express the non-equilibrium vibrational Helmholtz free energy A^*_{vib} in terms of the density of phonon states (the vibrational density of states) g(ω):

$$A^*_{vib} = \int_0^{\infty} \left[\frac{\omega}{2} + k_B T \ \mathrm{Ln}\left(1 - e^{-\frac{\omega}{k_B T}}\right)\right] g(\omega) d\omega \quad (9)$$

$$F^*(x, V; T) = E_{stat}(x, V) + A^*_{vib}(x, V; T) \quad (10)$$

where n represents the atoms number per unit volume, and D (θ/T) indicates the Debye integral, which is written as:

$$D(x) = \frac{3}{x^3} \int_0^x \frac{y^3 e^{-y}}{1 - e^{-y}} dy \quad (11)$$

To get the equilibrium state, we minimize Gibbs free energy G^* with respect to volume at constant pressure and temperature:

$$\left(\frac{\partial G^*(V, P, T)}{\partial V}\right)_{P,T} = 0 \quad (12)$$

Solving the last equation enable us to find formulas of various thermal quantities, such as: entropy (S), the heat capacity at constant volume (C_v), and the thermal expansion coefficient (α) which are given by:

$$S = -3nk_B \ln\left(1 - e^{-\theta_D/T}\right) + 4nk_B D(\theta_D/T) \quad (13)$$

$$C_v = 12nk_B D(\theta_D/T) - \frac{9nk_B \theta_D/T}{e^{\theta_D/T} - 1} \quad (14)$$

$$\alpha = -\frac{1}{V}\left(\frac{\partial V}{\partial T}\right)_P = \frac{\gamma C_V}{V B_T} \quad (15)$$

Heat capacity at volume constant C_v that is expressed by formula (2) depicts how much energy can be absorbed by 1 mol of compound when temperature increases by 1 K and is the result of vibrations of the atoms of lattice [42]. We plotted in Fig. 6 the variation of heat capacity of $CuYZ_2$ (Z = S, Se and Te) as a function of volume and pressure.

Fig. 12-a shown that at low temperature (smaller than 200 k) C_v increases with temperature and proportions to T^3, whereas it set up 100 j/mol. k) at a temperature equal or greater than 450 K which is in accordance to Petit Dulong law [43]. At ambient temperature (300 k), all studied compounds have high heat capacity values, where the greatest value was for $CuTe_2$ (96.47 j/mol.k) and the smallest value for $CuYS_2$ (91.89 j/mol.k). On the other hand, pressure affects the heat capacity C_v, where the curves C_v-P in Fig. 11-b appears a linear decrease of the heat capacities values with pressure increasing of all compounds.

We plotted in Fig. 13 the pressure and temperature effects on entropy thermal quantity and this latter means the unconvertible energy in system. According to Fig. 13-a, $CuYTe_2$ has higher entropy compared to the other compounds, also, the three curves of entropy change with increasing pressure and temperature and show a quasi-linear increase in entropy with increasing temperature and pressure for each of them separately. We can explain this observation as follow: the increase of temperature leads to a growth in the vibration modes and consequently the number of configurations possible while increasing pressure affects the atoms movement and therefore decreases the numbers vibrations atoms.

Thermal expansion expresses the proportion of change in dimension per unit degree temperature change at constant pressure when the temperature changes. Higher temperature leads to rise in the movement of the atoms that make up the substance and this leads to a change in its volume. Vibrations of the constituent atoms of the substance always play an important role and affected by external heat and their inter-atomic distances [44]. The coefficient of thermal expansion is related to several factors [45] such as the nature of its constituent atoms, the number of bonds, and the type of its structure. Fig. 14-a shows the variation of the coefficient of thermal expansion as a function of temperature. According to this figure, we can see that the thermal expansion of all studied compounds increases rapidly for temperatures less than 200 K and slowly for higher than 200 K. Also, we can notice that at temperatures less than 350 K, $CuYTe_2$ compound has the greatest thermal expansion coefficient, while at temperatures higher than 350 k the $CuYSe_2$ thermal expansion value become upper than the other.

The most important thermal property is the Debye temperature. It is associated with many mechanical and elastic properties, and it represents the temperature that caused the greatest number of vibration modes, Also, Debye temperature θ_D is associated to sound velocity due to the reason that vibrations of solid are considered as elastic waves [42, 46]. The obtained results of the temperature dependence of Debye temperature for all compounds $CuYZ_2$ (Z = S, Se and Te) are plotted in Fig. 14-b. Curves of θ_D-T exhibit a linear decreasing of Debye's temperature with increasing temperature where $CuYS_2$ has the highest value compared to $CuYTe_2$ and $CuYSe_2$ compounds.

3.5. Thermoelectric properties

To estimate Seebeck coefficient, electrical conductivity (σ/τ), the thermal conductivity (κ/τ) and electronic specific heat capacity (*c*) of $CuYZ_2$ compounds (Z = S,Se and Te) for different temperature (300, 500 and 700 k) in the first step as function of the relative chemical potential

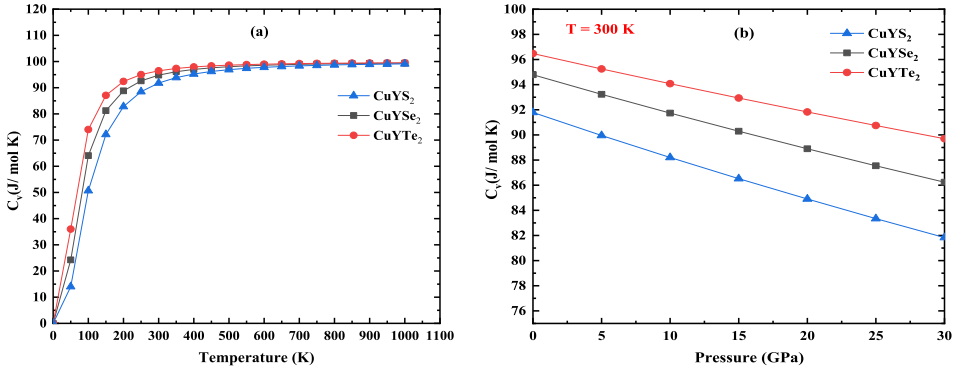

Fig. 12. Pressure and temperature dependence of heat capacity "C_v" on $CuYZ_2$ (Z = S, Se and Te) compounds.

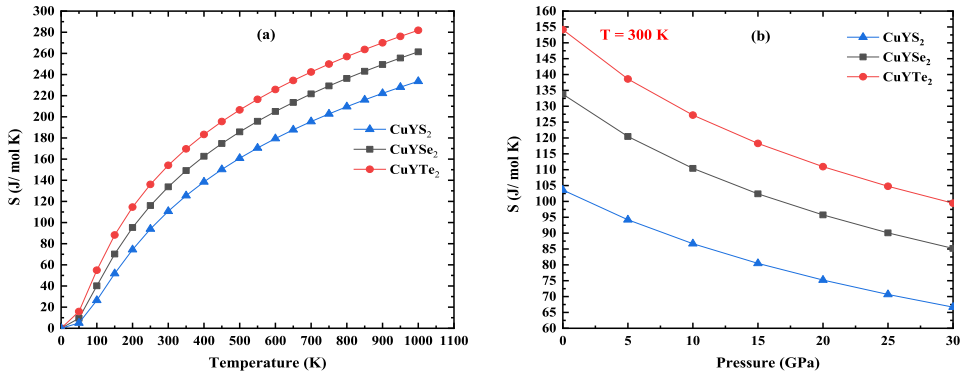

Fig. 13. Pressure and temperature dependence of entropy "S" of $CuYZ_2$ (Z = S, Se and Te) compounds.

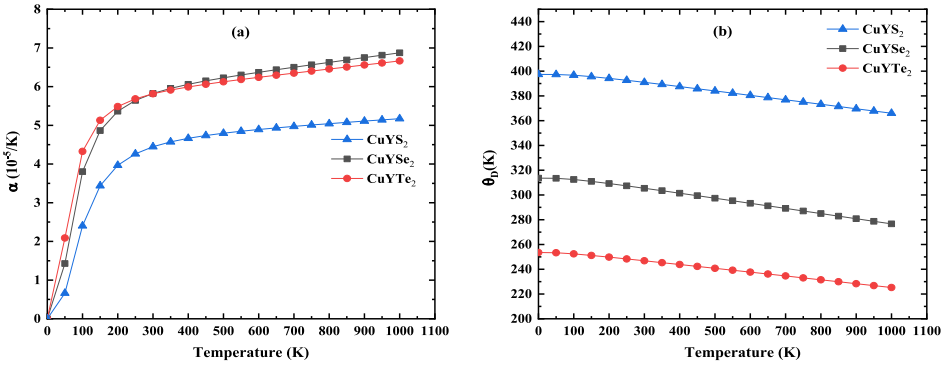

Fig. 14. Temperature dependence of entropy "S" of $CuYZ_2$ (Z = S, Se and Te) compounds.

where the positive value of chemical potential (μ) reveals that the doping is n-type whereas the negative value indicates the p-type doping [47], and at Fermi level for each $CuYZ_2$ (Z = S,Se and Te) compound at room temperature equal to 300 K we depend on the semi-classical Boltzmann transport theory implemented in BoltzTraP code [26].

The intrinsic Seebeck coefficient is the ratio of the voltage created between the ends of a material when its ends are exposed to a thermal gradient. This thermal gradient causes the moving charge carriers (electrons or holes) [48] and induced an electrical current.

We plotted in Figure (15-a) the variation of Seebeck coefficient along the relative chemical potential μ to the Fermi level μ_0 for all $CuYZ_2$ (Z = S, Se and Te) compounds at three temperatures values (300, 500 and 700 K). According to the obtained results, we can see at 300 K that the Seebeck coefficient is as great as possible for the three materials studied.

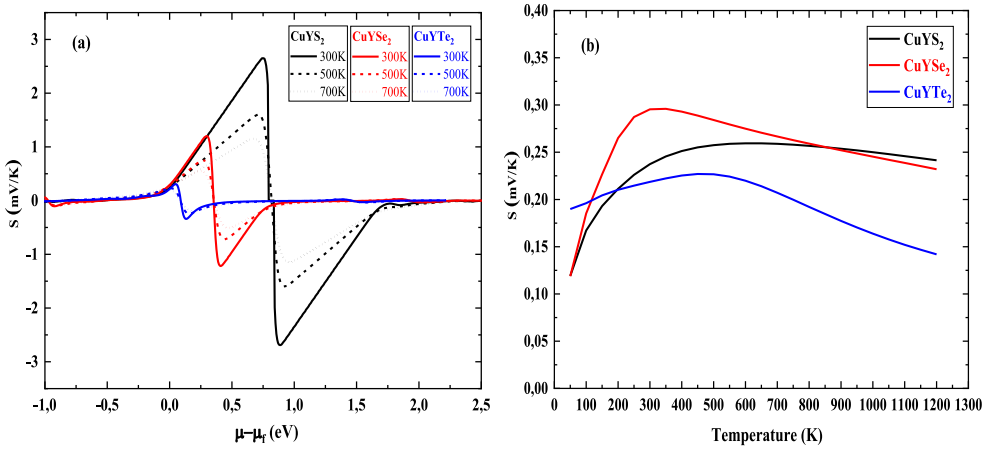

Fig. 15. Variation of Seebeck coefficient for $CuYZ_2$ (Z = S, Se and Te) as function of: (a) the relative chemical potential for different temperature values (300, 500 and 700 K). (b) As function temperature at Fermi level.

We can also see that the $CuYS_2$ compound has a significantly higher Seebeck coefficient than the other two compounds, with a maximum value set up 2.7 mV/K at 300 K and decreasing to 1.6 mV/K if the temperature increases to 700 K. Figure (15-b) shows the temperature variations of the Seebeck coefficient computed exactly at the Fermi level. The Seebeck coefficient rises to its maximum value at temperatures 650, 350 and 500 K for $CuYS_2$, $CuYSe_2$ and $CuYTe_2$ respectively, also we can see that the coefficient of Seebeck for the$CuYSe_2$ compound at room temperature is greater for the remaining compounds.

The other three important parameters in the study of thermoelectric phenomena are the electrical conductivity (σ/τ), electronic thermal conductivity (κ/τ) and electronic specific heat (c) of the free electrons in material where these factors express the contribution of the electrons movement to the conductivity of electric current, its contribution to thermal conductivity and its contribution to the heat capacity of the material, respectively. In Figs. 16–17 and 18, we have plotted the variation of the electrical conductivity (σ/τ) coefficient, the electronic thermal conductivity (κ/τ) and electronic specific heat (c) of $CuYZ_2$ in terms of chemical potential at different temperatures (300, 500 and 700 K) and as function of temperature at Fermi level.

The electrical conductivity, which is a measure of free charge-carrier flow of the material [49]. The electrical conductivity directly depends upon the carrier concentration (n) and mobility (μ) through the relation ($\sigma = ne\mu$) [47]. According to the results obtained about the changes of electrical conductivity in terms of the relative chemical potential at different temperatures (300, 500 and 700 K) shown in Fig. 16-a. We note that the $CuYTe_2$ compound has higher electrical conductivity than the rest compounds, where its maximum value was at the relative chemical potential in the range -1, -0.5 eV, also it can be noted that the electrical conductivity has the highest value at the temperature of 300 k and decreased slightly with increasing temperature for the all studied compounds, whereas the electrical conductivity of the $CuYS_2$ compound is large when the relative chemical potential is greater than 1.5eV. Fig. 16-b characterizes the electrical conductivity variation in terms of temperature for the three compounds at the Fermi level for each compound. The results indicate that electrical conductivity is non-existent at low temperatures and then goes up with increasing temperature, $CuYSe_2$ compound having a higher electrical conductivity coefficient than the other compounds.

It is usually known that the contributions of electrons to thermal and electrical conductivity are exactly proportional and related to each other by relation of Wiedemann–Franz law $\kappa = L\,\sigma\,T$ (L: Lorentz constant), so we can see similar shapes of curves for the electrical conductivity (σ/τ) and the electronic thermal conductivity (κ_e/τ) (see Fig. 17 (a and b)) where the increase of the electronic thermal conductivity is related to the electron-phonon interaction due to random transport carries [50].

The electronic heat capacity (c) is independent of system size and yields a degree of temperature change per unit of the substance by absorbing heat [49]. The variation of the electronic heat capacity (c) as function of the relative chemical potential at different temperatures (300, 500 and 700K) in both is shown in Fig. 18-a. The results indicated that the value of electronic heat capacity (c) takes higher values in the relative chemical potential range of -2 eV–0 eV for the three studied compounds, and the value of the capacity increases with rising temperature for the three compounds. The plotted curves also reveal that the $CuYS_2$ compound has a higher electronic heat capacity (c) than the other compounds unlike to $CuYTe_2$ compound that having the lowest values. Concerning the variations in electronic heat capacity (c) as a function of temperature computed at the Fermi level (See Fig. 18-b), we found that the electronic heat capacity (c) has zero values at temperatures below 150 K, whereas the electronic heat capacity (c) starts to rise as temperature increases and it increases more in $CuYS_2$ than $CuYTe_2$ and $CuYSe_2$.

Fig. 19 (a - b) display the variation of ZT factor as a function of chemical potential at different temperatures and as function of temperature at Fermi level for each compound. This parameter is used to express the qualification of materials to transfer heat into useful electric energy.

As previously mentioned, the efficiency of materials in converting heat into electricity varies from one material to another, as can be predicted theoretically by estimating the ratio of merit, this latter is related to the many other thermoelectric properties of the material such as the contribution of electrons to thermal conductivity,electrical conductivity in addition to Seebeck coefficient. To obtain a high merit ZT ratio, the material must have high Seebeck factor, high electricity fans and low thermal conductivity, which are significantly contributing to the heat energy transfer to electricity instead of storing or transported as a heat. According to Fig. 19-a shown to the ZT variation in term of the chemical potential at different temperatures, we note that both $CuYS_2$ and $CuYSe_2$ compounds have high ZT factor, unlike to $CuYTe_2$ compound. For the variations of ZT coefficient in terms of temperature at the Fermi level (see Fig. 19-b) we note that the coefficient value for the $CuYTe_2$ compound reaches a maximum at a temperature of 300 K and then decreases with increasing temperature, in contrast to $CuYS_2$ and $CuYSe_2$ compounds, where the coefficient value remains high and nearly constant at temperatures greater than 300 K.

4. Conclusion

Aspects of our work included estimation of structural, electronic and optical properties of copper-based chalcogenides: $CuYS_2$, $CuYSe_2$, and $CuYTe_2$ in orthorhombic and hexagonal structural phases using the first

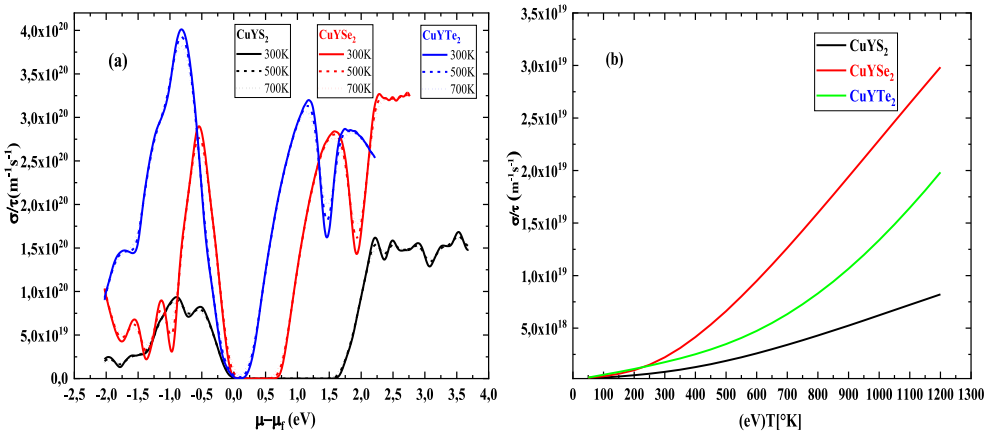

Fig. 16. Variation of electrical conductivity (σ/τ) for $CuYZ_2$ (Z = S, Se and Te) as function of: (a) the relative chemical potential for different temperature values (300, 500 and 700 K). (b) Temperature at Fermi level.

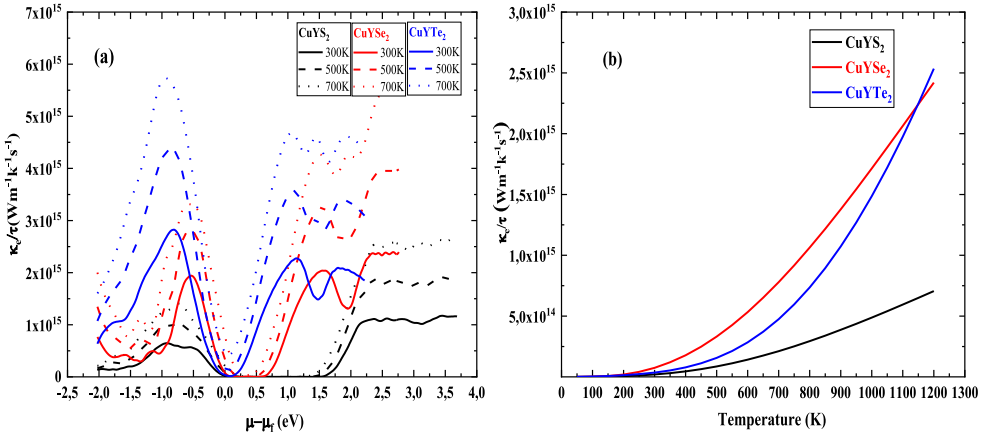

Fig. 17. Variation of electronic thermal conductivity (κ/τ) for $CuYZ_2$ (Z = S, Se and Te) as function of: (a) the relative chemical potential for different temperature values (300, 500 and 700 K), (b) temperature at Fermi level.

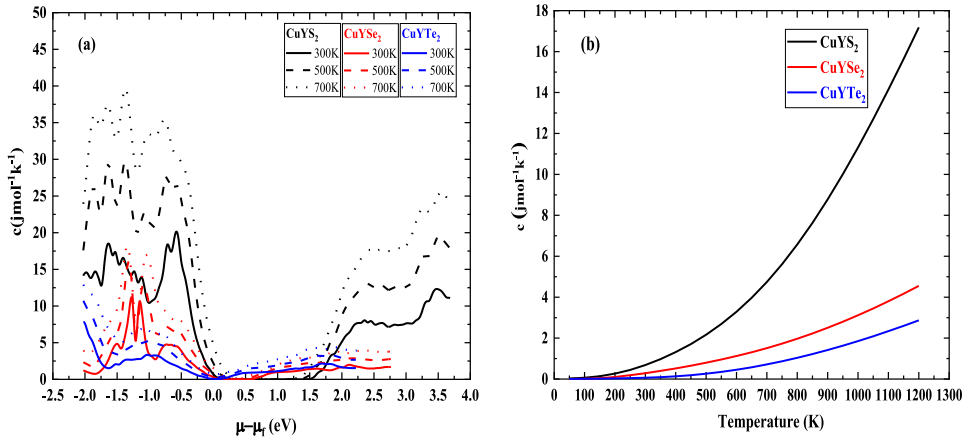

Fig. 18. Variation of electronic heat capacity (c) for $CuYZ_2$ (Z = S, Se and Te) as function of: (a) the relative chemical potential for different temperature values (300, 500 and 700 K). (b) Temperature at Fermi level.

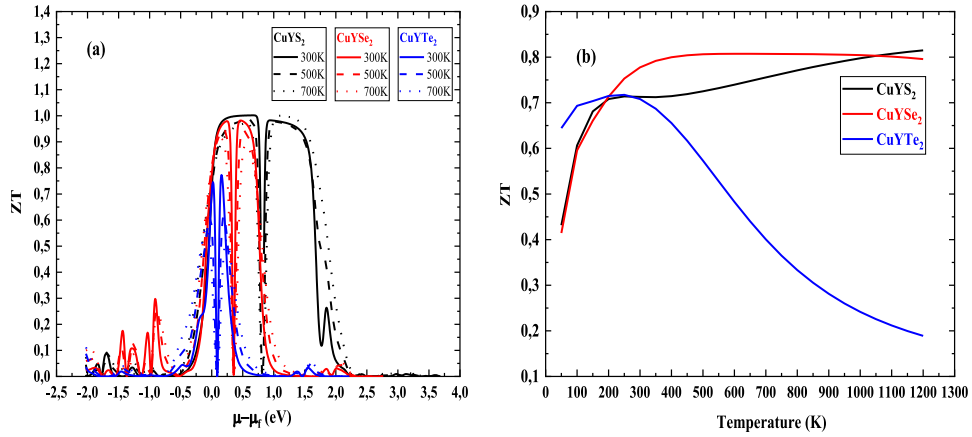

Fig. 19. Variation of (a) the merit figure (*ZT*) for $CuYZ_2$ (Z = S, Se and Te) as function of: (a) the relative chemical potential for different temperature values (300, 500 and 700 K). (b) Temperature at Fermi level.

principle calculation based on DFT theory. The analysis of the obtained results showed that the three compounds have the same electronic behavior, as they are semiconductors with different energy gaps. In addition, these compounds are considered to have good cohesive energies, especially $CuYS_2$ compound. Studying the optical properties indicates that the three compounds have good optical properties, in particular, $CuYS_2$ compound, which has a high absorption coefficient compared to the rest of the compounds. Which makes them candidate materials to use in photovoltaic applications. With regard to the temperature and pressure effects in the thermodynamic properties of the

three compounds, we found that the $CuYZ_2$ with the sulfur atom (S) has a less ability to absorb energy at ambient temperatures compared to the rest of the compounds as well as other thermal properties under the influence of pressure and heat, so our study appears that $CuYZ_2$ (Z = S, Se and Te) are promising compounds to use them in electro-optical fields and its applications. Estimating thermoelectric properties based on the semi-classical Boltzmann theory, such as thermal conductivity, Seebeck coefficient, and electronic conductivity, allows us to validate the ability of both $CuYS_2$ and $CuYSe_2$ to be used as thermoelectric materials due to its specific thermodynamic and electronic features. The thermoelectric findings indicate that $CuYS_2$ is a good candidate thermoelectric device due to their high Seebeck coefficient reaching to 3.0 mV/K and low thermal conductivity value at ambient temperature.

CRediT authorship contribution statement

Mohammed Elamin Ketfi: Conceptualization, Methodology, Writing and Investigation. **Hamza Bennacer:** Visualization, Investigation. **Saber Saad Essaoud:** Verification, Writing and Conducting a research and investigation process. **Mohamed Issam Ziane:** Supervision. **Abdelkader Boukortt:** Reviewing, Software.

Declaration of competing interest

The authors declare that they have no known competing financial interests or personal relationships that could have appeared to influence the work reported in this paper.

Acknowledgments

The Algerian Ministry of Higher Education and Scientific Research, as well as the General Directorate of Scientific Research and Technological Development, supported this work. All collaborators who participated in this work are deeply appreciated by the authors. Also, a lot of thanks to Dr LAADJAL Mohamed (University of M'sila, Algeria) for his beneficial discussions, as well as, Dr BENAISSA Cherif Youcef (University of Chlef, Algeria) and Dr HADJAB Moufdi (University of M'sila, Algeria) for their valuable guidance and discussions.

References

[1] H. Bennacer, A. Boukortt, S. Meskine, M. Hadjab, M.I. Ziane, A. Zaoui, First principles investigation of optoelectronic properties of $ZnXP_2$ (X= Si, Ge) lattice matched with silicon for tandem solar cells applications using the mBJ exchange potential, Optik 159 (2018) 229–244.
[2] J. Jiang, R. Giridharagopal, E. Jedlicka, K. Sun, S. Yu, S. Wu, Y. Gong, W. Yan, D. S. Ginger, M.A. Green, Highly efficient copper-rich chalcopyrite solar cells from DMF molecular solution, Nanomater. Energy 69 (2020) 104438.
[3] S. Garabagiu, G. Borodi, D. Marconi, Copper-based ternary chalcogenides thin films fabricated by PLD as potential thermoelectrics, Mater. Lett. 243 (2019) 125–127.
[4] L. Fu, Y. Guo, S. Zheng, Synthesis, crystal structure and optical properties of Ce doped $CuInSe_2$ powders prepared by mechanically alloying, J. Alloys Compd. 591 (2014) 304–307.
[5] S. Li, R. Ma, X. Zhang, X. Li, W. Zhao, H. Zhu, Copper yttrium selenide: a potential photovoltaic absorption material for solar cells, Mater. Des. 118 (2017) 163–167.
[6] L.D. Gulay, V.Y. Shemet, I.D. Olekseyuk, Crystal structures of the compounds $YCuS_2$, Y_3CuSnS_7 and $YCuPbS_3$, J. Alloys Compd. 388 (2005) 59–64.
[7] U. Aydemir, J.-H. Pöhls, H. Zhu, G. Hautier, S. Bajaj, Z.M. Gibbs, W. Chen, G. Li, S. Ohno, D. Broberg, $YCuTe_2$: a member of a new class of thermoelectric materials with $CuTe_4$-based layered structure, J. Mater. Chem. A. 4 (2016) 2461–2472.
[8] J.-H. Pöhls, Z. Luo, U. Aydemir, J.-P. Sun, S. Hao, J. He, I.G. Hill, G. Hautier, A. Jain, X. Zeng, First-principles calculations and experimental studies of XYZ_2 thermoelectric compounds: detailed analysis of van der Waals interactions, J. Mater. Chem. A. 6 (2018) 19502–19519.
[9] D. Huang, J.-W. Jiang, J. Guo, Y.-J. Zhao, R. Chen, C. Persson, Group-IV (Si, Ge, and Sn)-doped $AgAlTe_2$ for intermediate band solar cell from first-principles study, Semicond. Sci. Technol. 32 (2017), 065007.
[10] A. Sajid, S. Ullah, G. Murtaza, R. Khenata, A. Manzar, S.B. Omran, Electronic structure and optical properties of chalcopyrite $CuYZ_2$ (Y= Al, Ga, In; Z= S, Se): an ab initio study, J. Optoelectron. Adv. Mater. 16 (2014) 76–81.
[11] M.G. Brik, First-principles calculations of the structural, electronic, optical and elastic properties of the $CuYS_2$ semiconductor, J. Phys. Condens. Matter 25 (2013) 345802.
[12] J. Jiang, W. Zhou, Y. Xue, H. Ning, X. Liang, W. Zhou, J. Guo, D. Huang, Intermediate band insertion by group-IIIA elements alloying in a low cost solar cell absorber $CuYSe_2$: a first-principles study, Phys. Lett. 383 (2019) 1972–1976.
[13] M. Kumar, C. Persson, $CuSbS_2$ and $CuBiS_2$ as potential absorber materials for thin-film solar cells, J. Renew. Sustain. Energy 5 (2013), 031616.
[14] M. Hadjab, J.-M. Wagner, F. Bouzid, S. Boudour, A. Hadj Larbi, H. Bennacer, M. I. Ziane, M.A. Saeed, H. Abid, S. Berrah, A numerical optimization study of CdS and $Mg_{0.125}Zn_{0.875}O$ buffer layers in CIGS-based solar cells using wx AMPS-1D package, Int. J. Model. Simulat. (2021) 1–13.
[15] M.I. Ziane, M. Tablaoui, A. Khelfane, M. Hadjab, H. Bennacer, Optoelectronic properties of the new quaternary chalcogenides $Zn_2CuInTe_4$ and $Cd_2CuInTe_4$: ab-initio study, Optik 157 (2018) 248–258.
[16] M.I. Ziane, D. Ouadjaout, M. Tablaoui, R. Nouri, W. Zermane, A. Djelloul, H. Bennacer, A. Mokrani, M. Hadjab, H. Abid, First-principle computed structural and thermodynamic properties of $Cu_2ZnSn(S_xSe_{1-x})_4$ pentanary solid solution, J. Electron. Mater. 48 (2019) 6991–7002.
[17] S. Adachi, Earth-abundant Materials for Solar Cells: Cu_2-II-IV-VI_4 Semiconductors, John Wiley & Sons, 2015.
[18] S.R. Kodigala, $Cu(In_{1-x}Ga_x)Se_2$ Based Thin Film Solar Cells, Academic Press, 2011.
[19] T. Gao, Q. Zhang, L. Li, X. Zhou, L. Li, H. Li, T. Zhai, 2D ternary chalcogenides, Adv. Opt. Mater. 6 (2018) 1800058.
[20] P. Blaha, K. Schwarz, G.K. Madsen, D. Kvasnicka, J. Luitz, Augment wien2k, Plane wave local orbitals program calc, Cryst. Prop. (2001).
[21] W. Kohn, L.J. Sham, Self-consistent equations including exchange and correlation effects, Phys. Rev. 140 (1965) A1133.
[22] J.P. Perdew, K. Burke, M. Ernzerhof, Generalized gradient approximation made simple, Phys. Rev. Lett. 77 (1996) 3865–3868.
[23] A.D. Becke, E.R. Johnson, A Simple Effective Potential for Exchange, American Institute of Physics, 2006.
[24] V.L.A. Otero-de-la-Roza, D. Abbasi-Pérez, Gibbs2: a new version of the quasiharmonic model code. II. Models for solid-state thermodynamics, features and implementation, Comput. Phys. Commun. 182 (10) (2011) 2232–2248.
[25] V.L.A. Otero-de-la-Roza, Gibbs2, A new version of the quasi-harmonic model code. I. Robust treatment of the static data, Comput. Phys. Commun. 182 (8) (2011) 1708–1720.
[26] G.K. Madsen, D.J. Singh, BoltzTraP. A code for calculating band-structure dependent quantities, Comput. Phys. Commun. 175 (2006) 67–71.
[27] C.G. Broyden, The convergence of a class of double-rank minimization algorithms 1. general considerations, IMA J. Appl. Math. 6 (1970) 76–90.
[28] C.G. Broyden, The convergence of a class of double-rank minimization algorithms: 2. The new algorithm, IMA J. Appl. Math. 6 (1970) 222–231.
[29] F.D. Murnaghan, The compressibility of media under extreme pressures, Proc. Natl. Acad. Sci. U.S.A. 30 (1944) 244.
[30] P. Lauxmann, T. Schleid, $CuYS_2$: ein ternäres Kupfer (I)-Yttrium (III)-Sulfid mit Ketten $^1{}_\infty\{[Cu(S1)_{3/3}(S2)_{1/1}]^{3-}\}$ cis-kantenverknüpfter $[CuS_4]^{7-}$-Tetraeder, Z. Anorg. Allg. Chem. 626 (2000) 1608–1612.
[31] P. Villars, H. Okamoto, Springer-verlag berlin heidelberg & material phases data system (MPDS), Switz. Natl. Inst. Mater. Sci. NIMS Jpn. (n.d.).
[32] M.D. Heinemann, F. Ruske, D. Greiner, A.R. Jeong, M. Rusu, B. Rech, R. Schlatmann, C.A. Kaufmann, Advantageous light management in $Cu(In, Ga)Se_2$ superstrate solar cells, Sol. Energy Mater. Sol. Cells 150 (2016) 76–81.
[33] M.A. Khan, A. Kashyap, A.K. Solanki, T. Nautiyal, S. Auluck, Interband optical properties of Ni 3 Al, Phys. Rev. B 48 (1993) 16974.
[34] Optical Properties of Materials and Their Applications, second ed. | Wiley, Wiley. Com. (n.d.). (accessed February 4, 2021).
[35] C. Ambrosch-Draxl, J.O. Sofo, Linear optical properties of solids within the full-potential linearized augmented planewave method, Comput. Phys. Commun. 175 (2006) 1–14.
[36] M. Gajdoš, K. Hummer, G. Kresse, J. Furthmüller, F. Bechstedt, Linear optical properties in the projector-augmented wave methodology, Phys. Rev. B 73 (2006), 045112.
[37] B.U. Haq, S. AlFaify, A.S. Jbara, R. Ahmed, F.K. Butt, A. Laref, A.R. Chaudhry, Z. A. Shah, Optoelectronic properties of three PbSe polymorphs, Ceram. Int. 46 (2020) 22181–22188.
[38] A.S. Jbara, Z. Othaman, H.A. Aliabad, M.A. Saeed, Electronic and optical properties of γ-and-Alumina by first principle calculations, Adv. Sci. Eng. Med. 9 (2017) 287–293.
[39] A.S. Jbara, J. Munir, B.U. Haq, M.A. Saeed, Density functional theory study of mixed halide influence on structures and optoelectronic attributes of $CsPb(I/Br)_3$, Appl. Opt. 59 (2020) 3751–3759.
[40] H. Tributsch, Solar energy-assisted electrochemical splitting of water. Some energetical, kinetical and catalytical considerations verified on MoS_2 layer crystal surfaces, Z. Naturforsch. 32 (1977) 972–985.
[41] T. Kaur, B. Kaur, B.H. Bhat, S. Kumar, A.K. Srivastava, Effect of calcination temperature on microstructure, dielectric, magnetic and optical properties of $Ba_{0.7}La_{0.3}Fe_{11.7}Co_{0.3}O_{19}$ hexaferrites, Phys. B Condens. Matter 456 (2015) 206–212.
[42] V. Srivastava, N. Kaur, X. Wang, M. Mushtaq, S.A. Dar, First-principles study on structural, electronic, magnetic, elastic, mechanical and thermodynamic properties of Mn_2PtCo Heusler alloy, Int. J. Energy Res. 45 (2021) 11305–11319.
[43] P.L. Dulong, A.-T. Petit, Recherches sur quelques points importans de la theorie de la Chaleur, 1819.
[44] V. Srivastava, N. Kaur, R. Khenata, S.A. Dar, Investigation of the electronic, magnetic, elastic, thermodynamic and thermoelectric properties of Mn_2CoCr Heusler compound: a DFT-based simulation, J. Magn. Magn Mater. 513 (2020) 167107.

[45] I. Jum'h, H. Baaziz, Z. Charifi, A. Telfah, Electronic and magnetic structure and elastic and thermal properties of Mn 2-based full heusler alloys, J. Supercond. Nov. Magnetism 32 (2019) 3915–3926.
[46] S.S. Essaoud, A.S. Jbara, First-principles calculation of magnetic, structural, dynamic, electronic, elastic, thermodynamic and thermoelectric properties of Co_2ZrZ (Z= Al, Si) Heusler alloys, J. Magn. Magn Mater. (2021) 167984.
[47] J. Singh, K. Kaur, S.A. Khandy, S. Dhiman, M. Goyal, S.S. Verma, Structural, electronic, mechanical, and thermoelectric properties of LiTiCoX(X= Si, Ge) compounds, Int. J. Energy Res. (2021).
[48] A. Telfah, S.S. Essaoud, H. Baaziz, Z. Charifi, A.M. Alsaad, M.J.A. Ahmad, R. Hergenröder, R. Sabirianov, DFT investigation of physical properties of KCrZ (Z=S, Se, Te) half-heusler alloys. Phys. Status Solidi B n/a (n.d.).
[49] S.A. Khandy, D.C. Gupta, Structural, elastic and thermo-electronic properties of paramagnetic perovskite $PbTaO_3$, RSC Adv. 6 (2016) 48009–48015.
[50] S.A. Khandy, J.-D. Chai, Strain engineering of electronic structure, phonon, and thermoelectric properties of p-type half-Heusler semiconductor, J. Alloys Compd. 850 (2021) 156615.